Journal of Power Sources 273 (2015) 368–374

Contents lists available at ScienceDirect

Journal of Power Sources

journal homepage: www.elsevier.com/locate/jpowsour

Electrochemical response in aprotic ionic liquid electrolytes of TiO_2 anatase anodes based on mesoporous mesocrystals with uniform colloidal size

Jose Manuel Amarilla [a, *], Enrique Morales [b], Jesus Sanz [a], Isabel Sobrados [a], Pedro Tartaj [a, *]

[a] Instituto de Ciencia de Materiales de Madrid, CSIC, Campus Universitario de Cantoblanco, 28049 Madrid, Spain
[b] Instituto de Ciencia y Tecnologia de Polimeros, CSIC, C/Juan de la Cierva 3, 28006 Madrid, Spain

HIGHLIGHTS

- Safe and stable Li-ion battery anodes from porous mesocrystals and ionic liquids.
- Wetting of 3–4 nm mesoporosity is possible by ionic liquid electrolytes.
- Colloidal mesocrystals can be easily processed as anode composites.
- Uniform mesoporous colloidal mesocrystals of TiO_2 anatase.

GRAPHICAL ABSTRACT

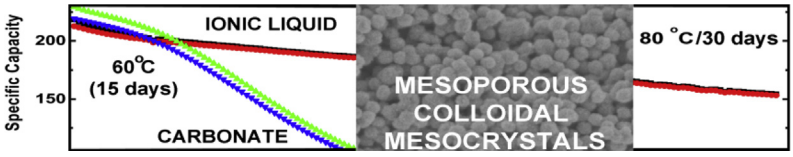

ARTICLE INFO

Article history:
Received 3 August 2014
Received in revised form
11 September 2014
Accepted 16 September 2014
Available online 28 September 2014

Keywords:
Li-ion batteries
TiO_2 anatase anodes
Mesocrystals
Mesoporous materials
Ionic liquids

ABSTRACT

Mesocrystals (superstructures of crystallographically-oriented inorganic nanocrystals) represent sophisticated configurations generated from biomineralization processes, and an example of nonclassical crystallization mechanisms. Being the closest relatives to single-crystals at the nanoscale, porous mesocrystals are considered as ideal configurations to improve functional properties, and to correlate structural and textural features with materials functionality. Here we show that TiO_2 anatase mesoporous colloidal mesocrystals, synthesized by a self-assembly/seeding method, can be easily processed as active materials in anode composites. These anode composites can be efficiently infiltrated during battery operation with safe aprotic ionic liquid electrolytes down to the mesoporosity of mesocrystals (3–4 nm), and operate over a wider temperature window than organic carbonates. For example, after continuous galvanostatic cycling for 1 month at high temperatures (15 days at 60 °C + 15 days at 80 °C, ~130 cycles), these anode composites sustain a capacity at 67 mA g^{-1} that is still remarkable for TiO_2-based anodes (155 mAh g^{-1} or 200 mAh cm^{-3}, coulombic efficiency of ~99%). On contrast, in organic carbonates the capacity decays down to 80 mAh g^{-1} after only 15 days at 60 °C. Our results suggest that the principles derived from porous anatase mesocrystal/ionic liquid electrolyte combinations could constitute the basis for battery applications in which safety, durability and variability in operating temperature represent the primary concerns.

1. Introduction

From laptops to cell phones, tablets and electric cars, lithium-ion rechargeable batteries (LiBs) have provided the energy required for portability since its commercial introduction by Sony in 1991. While there is a continuous interest in building batteries

* Corresponding authors.
E-mail addresses: amarilla@icmm.csic.es (J.M. Amarilla), ptartaj@icmm.csic.es (P. Tartaj).

http://dx.doi.org/10.1016/j.jpowsour.2014.09.106
0378-7753/

with enhanced power and energy densities, safety hazards imposed severe restrictions to any development in this direction. In fact, safety concerns forced the replacement of lithium metal by intercalation anodes (graphite) despite their much lower capacity (3860 vs 370 mAh g^{-1}). Safety concerns also limit the packing of components, which is a rather simple approach to enhance energy density in batteries. Among safety hazards, flammability and volatility associated with the electrolytes (organic carbonate solvents), and concerns on graphite anodes (electrodeposition of metallic lithium) demand for different approaches to reduce these risks [1–4]. Furthermore, there is also interest in extending the LiBs operating temperature because the organic carbonate electrolytes set a relatively low upper limit for efficiency, as they degrade above 50 °C [5].

TiO_2 anatase represents a safe and stable alternative to graphite [4,6]. Anatase operates at high voltages (>1 V vs. Li/Li^+), and less emphasized is the fact that during battery cycling, the difference in density between non-lithiated and lithiated phases is only 1–2% (structural integrity preserved as expansion-contraction during operation is negligible). Aside from solid-state electrolytes or hybrid compositions, aprotic ionic liquids (AILs) represent a safer and tested alternative to organic carbonates in LiBs [1,7–10]. Recent reports indicate the potential of using protic ionic liquids (PILs) instead AILs, at least for cathodes [11,12], but we understand these liquids are not sufficiently tested, for example, against temperature stability of bounded protons.

Batteries built from anatase anodes and AILs must be intended for applications in which safety, durability and variability in operating temperature represent the primary concerns. On the one hand, anatase anodes when compared to graphite have lower energy density (among others, the voltage difference between this anode and the corresponding cathode in a battery is of course significantly lower). On the other hand, rate capabilities are limited by lithium ion transport when using the currently available AILs as solvents for battery electrolytes [1,2,7–9,13–17]. Partial mixing of AILs with organic carbonates seems a good alternative to improve rate capabilities while expanding operating temperatures [10]. However, we understand that being safety the primary concern, working with only AILs should be preferred. For example, vaporization of the organic carbonate component could be still possible, and could cause the break of the battery by excessive internal pressure with further leakage of contaminants. Besides, we are especially interested in confirming the wettability under battery operating conditions of the mesocrystals here reported by the AILs at their mesoporous scale size (3–4 nm, see details below), and wall effects do not assure similar wettability by every component of a mixture at these porous sizes. The issue of wettability though less emphasized than that of limited lithium transport represents a real challenge, as viscosity is high in available AILs electrolytes for LiBs [1,16]. In our electrode, as we describe in the Results and discussion section, we have three porosity scales and wetting efficiency will be reached if all of that porosity is filled with the AIL electrolyte.

The interest in mesocrystals have emerged from fundamental studies in both biomineralization processes and nonclassical crystallization mechanisms [18,19]. As single-like crystals with nanostructural features, the last five years have seen significant examples of their applicability in energy applications [20–30]. These nanostructures when compared to other advanced configurations can combine good textural properties with good crystallinity. As most of the energy applications require materials with high surface area (high number of active sites), surface degradation can be minimized if high surface area materials are complemented with good crystallinity. Furthermore, for those applications in which extensive processing of active materials is required (batteries for example), limiting the size of mesocrystals to the colloidal domain opens an avenue to a wide variety of standard processing techniques [24].

Some of us have recently established that self-assembly combined with seeding represents a versatile route to synthesize mesocrystals with different colloidal sizes and good textural properties [31], and that some of these mesocrystals can be used in combination with organic carbonate electrolytes to produce efficient anodes [29].Here we report that optimized TiO_2 anatase porous colloidal mesocrystals synthesized using this method can be easily processed as active materials in anode composites, and when combined with aprotic ionic liquids, can simultaneously lower LiBs risks and expanding their operating temperature.

2. Experimental

2.1. Mesocrystals synthesis

The porous anatase mesocrystals for this study were prepared following a synthesis method that combines thermally-driven self-assembly of nanomicelles with seeding-assisted chemistry [29,31]. In a typical experiment carried out in 500 mL Schott capped glass bottles (total reaction volume of 400 mL), 35.3 g of Igepal Co-520 (Aldrich) were dissolved in 175 mL of cyclohexane (Aldrich) under magnetic stirring. Then, 9.5 mL of $TiOSO_4$ (1.25 M solution in H_2SO_4, Aldrich) and 12 mL of distilled H_2O were injected into the solution under strong magnetic stirring in the form of fourth aliquots separated by a 30 min time interval. Each aliquot injection consisted itself in the alternate injection of $TiOSO_4$ and H_2O in three consecutives aliquots. After the addition of the 9.5 mL of $TiOSO_4$ and the 12 mL of distilled H_2O, we added another 175 mL of cyclohexane and then the resulting solution was typically left overnight under magnetic stirring to assure the formation of a good microemulsion. To this transparent microemulsion, we added 3 mL of a sol containing the anatase seeds (0.2 M) in the form of fourth aliquots separated by 30 min intervals. The sol containing the nanoseeds was obtained by slowly adding 5.2 mL of $TiCl_4$ to 200 mL of water at 4 °C under vigorous stirring and further dialysis [32].After seeds addition to the microemulsion, the resulting suspension was stirred for another 1 h, and introduced in an oven set at 60 °C. After 20 h, the temperature of the oven was raised to 80 °C and kept for 72 h. Finally, the product was removed from the oven, washed several times with EtOH, dried at 50 °C and heated in air at 250 °C/24 h.

2.2. Characterization

2.2.1. Preparation and NMR characterization of the ionic liquid electrolyte

N-methyl-(n-butyl)pyrrolidinium bis(trifluoromethanesulfonyl) imide ionic liquid ($Pyr_{14}TFSI$), with a water content below 20 ppm, was obtained from Merck and used as received. Lithium bis(trifluoromethanesulfonyl)imide (LiTFSI), was obtained by 3 M (Fluorad HQ-115). The salt was dried under vacuum (24 h, 80 °C) prior to its use. Different concentrations of $Pyr_{14}TFSI$-LiTFSI electrolyte were prepared by dissolving the lithium salt in the ionic liquid. All operations and handling were carried out in an argon-filled glove box, with a humidity level below 1 ppm. The lithium-ion transport in the ionic liquid was analyzed by NMR (Bruker 400 MHz Avance, 9.4T). Specifically, lithium-ion diffusion coefficients were measured by using a pulsed field gradient method. In order to carry out precise measurements using this method, the echo signal must be firstly optimized to obtain adequate intensity. For our liquids the optimization of echo intensity required time intervals of 20 ms between field gradient pulses and pulses time of 2 ms. Once these parameters are set, the diffusion coefficient can be derived from the

variation of the echo signal intensity with the intensity of the pulsed field gradient by using a non-linear least square iterative method.

2.2.2. Electrodes processing

Composite electrodes were fabricated by dispersing anatase mesocrystals or commercial samples (80% by weight), carbon black (10 wt. %) (TIMREX Super-P) and the polyvinylidene fluoride binder (10 wt. %) (Mw ~534000, Aldrich) in 1-methyl-2-pyrrolidinone (Aldrich). The resulting slurry was stirred during 24 h and casted on the current collector (a cooper foil) using a doctor Blade (specifically the blade was set at a 200 μm height). Electrodes with a surface area of 1.13 cm^2 and ca. 1 mg of active material were firstly dried at 80 °C for 2 h and then at 120 °C under vacuum overnight. Finally, the dried electrodes were transferred to an argon globe box (H_2O content < 1 ppm) for cells assembly.

2.2.3. Structural and textural characterization

Phase identification was performed by X-ray diffraction analysis using a Bruker D8 Advance instrument (CuKα radiation, 40 kV, 30 mA). The crystal domain size was determined from the X-ray profiles using the Scherrer equation. The morphology, particle size and crystallinity of the mesocrystals were examined by transmission electron microscopy (TEM, 2000 FX2, JEOL), high-resolution transmission electron microscopy (HR-TEM, 300, JEOL) and field emission scanning electron microscopy (FE-SEM, Hitachi, SU 8000). Size parameters were evaluated from the images by counting around 100 particles. Nitrogen adsorption and desorption isotherms were performed at −196 °C in a Micromeritics ASAP 2010 volumetric adsorption system. The BET surface area was deduced from the analysis of the isotherm at low pressures (0.04–0.20) while pore size distributions were estimated using the BJH model. The microstructure and thickness of composite electrodes were evaluated by the same FE-SEM above-mentioned. The average thickness of the electrodes was also determined over an area of 1 cm^2 with a DUALSCOPE 90 from Fischer. Basically, this equipment used eddy currents to determine thicknesses.

2.2.4. Electrochemical characterization

The electrochemical properties of anatase were evaluated against a lithium-metal foil counter electrode (it also acts as reference electrode) using galvanostatic cycling tests in a cell voltage window between 2.7 and 1.0 V vs Li/Li^+. Charge current in all experiments was set to 67 mA g^{-1}. These tests were carried out with an Arbin-BT4 battery system using coin-type cell configurations (size 2032). A Whatman BSF-80 glass fibber was used as separator and as electrolyte either the ionic liquid electrolyte above-mentioned or a 1 M $LiPF_6$ solution in anhydrous mixtures of ethylene carbonate and dimethyl carbonate (1:1 weight ratio). Cells were assembled in an argon glove box (H_2O content < 1 ppm). The electrochemical measurements were conducted under thermostatic conditions at different temperatures (30, 60 and 80 °C). Importantly, the experiments were carried out at 30 °C instead room temperature because our temperature controller operates better at this slightly higher temperature.

Electrochemical impedance measurements were performed using a Biologic VMP3 multichannel battery tester equipped with the Electrochemical Impedance Spectrosocopy (EIS) board. Spectra were recorder at room temperature over a frequency range from 700 kHz to 0.1 Hz. The amplitude of ac signal was 5 mV, and the cells were measured at the constant potential of the cell after the appropriate equilibration; i.e. until no variation of the OCV was observed.

3. Results and discussion

3.1. Mesocrystals and films characterization

Fig. 1 shows the optimized anatase porous colloidal mesocrystals used in this report that were prepared by a self-assembly/seeding synthetic route (see Experimental section for details). Basically, the mesocrystals are monodisperse colloids (43 nm, SD = 4) with good textural properties (210 m^2 g^{-1}, mesoporosity ≈ 3.5 nm), made from oriented 6–7 nm anatase subunits. Importantly, the ~40 nm mesocrystals used in this study represent an optimization of previously reported sizes in terms of synthesis efficiency and electrochemical performance [29]. These mesocrystals are able to keep a similar electrochemical response in organic carbonates when compared to those of the best early reported (25 nm) [29], while being derived from compositions in which efficiency is doubled (see Experimental section and Fig. S1 in Supplementary information for details). Back to the central point of

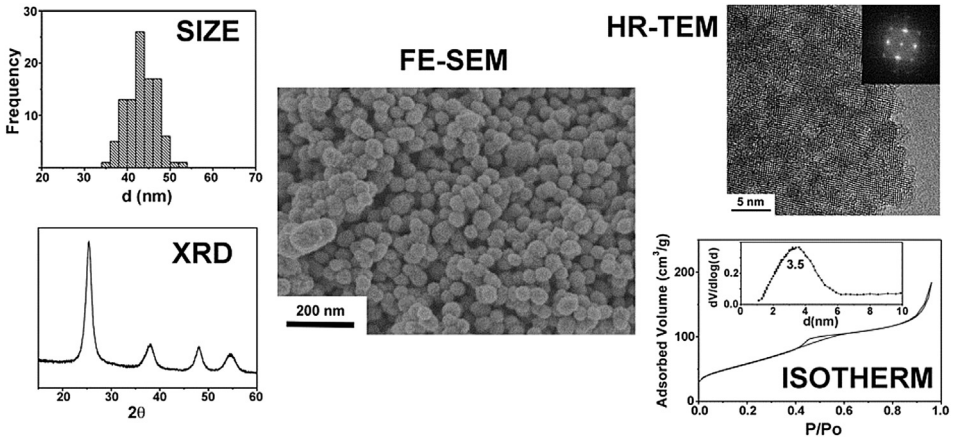

Fig. 1. The FE-SEM image and the corresponding size histogram show monodisperse spherical particles of colloidal size (43 nm, standard deviation = 4). XRD indicates that the particles are made from anatase subunits with a crystal size of around 6–7 nm (rigorously average size of a domain that diffracts coherently). According to HR-TEM and the corresponding FFT image (Inset), the anatase nanocrystals appear aligned in a preferential direction over an extensive area of the colloidal aggregate. Importantly, the texture of the particle can make some areas of the particle to appear misaligned or even with some apparent disorder. Together all of these techniques indicate that we have inorganic anatase nanocrystals oriented to form a superstructure with a size of ~40 nm (i.e. we have colloidal mesocrystals of anatase). The mesoporosity (~3.5 nm) of the mesocrystals is confirmed through the analysis of the N_2 isotherm and the pore size distribution (Inset).

this study, the good textural properties of the ~40 nm mesocrystals (good accessibility) together with the colloidal size (feasibility to be processed using widely established processing technologies) suggest that they can be used in combination with AIL electrolytes (LiTFSI 0.2M/PYR_{14}TFSI) to build safer and temperature stable LiBs. LiTFSI 0.2M/PYR_{14}TFSI was selected as electrolyte because is commercially available, and shows good electrochemical and temperature stability under battery operating conditions for LiTFSI concentrations around 0.1–0.3 M [10]. However, they have high viscosity and show limited lithium-ion transport. Therefore, we understand the good accessibility and processability of the mesocrystals here reported are essential for a better electrochemical performance. Recent reports of anatase nanotubes with a free volume around 70% (15 nm anatase walls and 70–100 nm hole diameter) indicate that good accessibility is essential when working with ionic liquids [17]. Importantly, the mesocrystals here reported have a density around 60% of the theoretical value (~40% of free volume, see Supplementary information for estimation). As we better describe below, this free volume assures good accessibility with indeed a higher intrinsic volumetric capacity than that of nanotubes.

As colloidal mesocrystals need to be processed in order to obtain functional electrodes, anode composites were prepared in a film configuration using standard processing techniques to come closer to technological approaches. Thus, carbon black and polyvinylidene fluoride were used as additives, and Dr. Blade was used for films preparation (see Experimental section). Fig. 2 shows that the electrodes consist of aggregates (0.5–5 μm) of well-preserved TiO_2 anatase spherical mesocrystals, and that even the largest aggregates retain significant intra-aggregate porosity. As above-mentioned the viscosity is high in the AILs here selected, so keeping in mind that according to Figs. 1 and 2 the composite electrodes have three porosity scales (mesocrystals' mesoporosity, intra- and interstitial aggregate porosities), wetting during battery operation is a relevant issue that we analyze in the next section.

3.2. Electrochemical response of mesocrystals in aprotic ionic liquid electrolytes

Fig. 3 shows the first five voltage curves at a rate of 67 mA g^{-1} for the mesocrystals and a commercial nanoanatase (25 nm from Aldrich) in both ionic liquid electrolytes and organic carbonate electrolytes. These curves are highly illustrative as they provide information on the lithium uptake mechanism and irreversibility processes, and in our system, provide confirmation on efficient wetting at all porous scales.

During battery operation poor wetting of ionic liquid electrolytes is usually manifested by an increase in specific capacity at full discharge during the first galvanostatic cycles (wetting progresses during measurement) followed by the usual decay [1,16]. In Fig. 3 we show in the ionic liquid electrolytes, the usual decay (analysis of this decay is described below) in specific capacity at full discharge during the first cycles for anodes made of mesocrystals or commercial nanoanatases with a thickness of ~6 μm and similar density. Efficient wetting, thus, is assured at least at intra- and interstitial aggregate porosities in electrodes of this thickness. Our results indicate that efficient wetting by the ionic liquid electrolytes also takes place at mesocrystals' mesoporous scale (3–4 nm). This conclusion is obtained after comparing the electrochemical performance of the ~40 nm mesocrystals with that of ~25 nm non-porous commercial nanoanatases in the composite anodes. The specific capacity at full discharge of anatase anodes strongly increases with the decrease on the anatase crystal size [33–37]. Thus, in infiltrated 40 nm mesocrystals the “electrochemical size” of anatase should be around the diameter of anatase subunits (6–7 nm) while in non-infiltrated mesocrystals it should be around 40 nm. On contrast, for the 25 nm non-porous commercial samples the “electrochemical size” should be logically around 25 nm (size is between that of infiltrated and non-infiltrated mesocrystals). Fig. 3 clearly shows that the capacity of mesocrystals in AILs at full discharge is better than even that of a commercial sample in carbonates at a current rate where lithium transport does not seem to

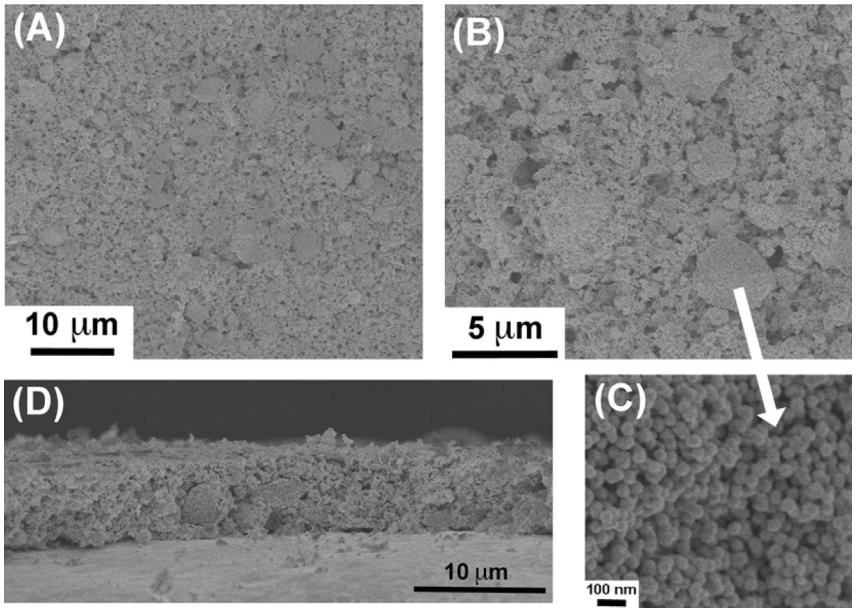

Fig. 2. (A), (B), and (C) are FE-SEM images of the electrodes top surface at different magnifications. The electrode consists of aggregates (0.5–5 μm) of well-preserved TiO_2 anatase spherical mesocrystals. The high-magnification image also shows that even the largest aggregates retain significant intra-aggregate porosity. (D) Lateral section of the electrode showing an area with a thickness around 5–6 μm deposited onto the Cu current collector. This thickness matches the average thickness determined over an area of ~1 cm^2 (6 ± 2 μm) using eddy currents technology (see Experimental section for details).

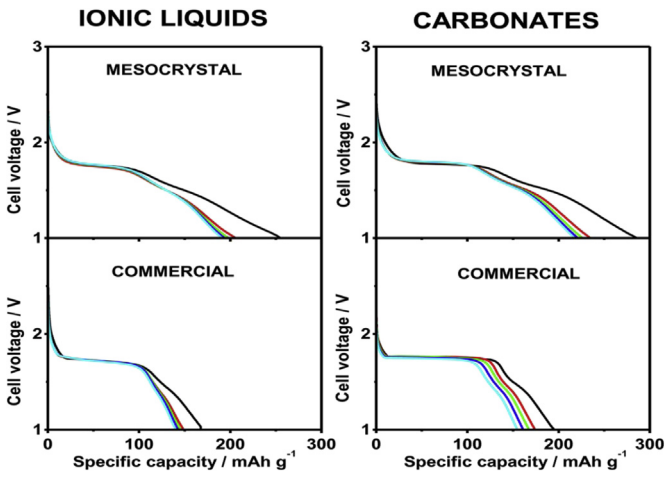

Fig. 3. Cell voltage curves (2.7–1.0 V vs Li/Li$^+$) measured at 30 °C (first five cycles from black to light blue) at a charge/discharge current of 67 mA g^{-1} for mesocrystals and 25 nm commercial nanoanatases in ionic liquid electrolytes (LEFT) and carbonate electrolytes (RIGHT). Importantly, experiments were carried out at 30 °C instead room temperature because our temperature controller operates better at this slightly higher temperature. (For interpretation of the references to colour in this figure legend, the reader is referred to the web version of this article.)

represent a relevant issue (67 mA g^{-1}). We can, therefore, assume that significant wetting also occurs at mesoporous scale (the anatase subunits with a 6–7 nm size are active for electrochemical insertion).

Fig. 3 also shows for all anodes, the three distinctive regions that have been associated with different electrochemical processes. The pre-plateau and plateau regions are mainly associated with the lithium uptake by the tetragonal anatase structure and a phase transformation to an orthorrombic lithiated phase, respectively [33]. In the post-plateau region, the lithium uptake by the orthorrombic phase progresses but also formation of a SEI (solid–electrolyte interface) can take place [33,37]. Moreover, there are significant reports that in this post-plateau region, surface or close to surface redox reactions contribute to the electrochemical response, especially when dealing with small nanoanatases [38–40]. In fact, the post-plateau profile is the typical observed on battery electrode materials at the nanoscale, and widely accepted to be related to these surface redox reactions (pseudocapacitor-like behavior) [41]. In accordance, the porous mesocrystals that have a higher surface area available for electrochemical reactions than that of non-porous 25 nm commercial samples, always show a more extended post-plateau region (Fig. 3).

Fig. 3 also shows that the significant irreversibility after the first discharge curve occurs both in carbonates and AILs at cut-off potentials between 1 and 2.7 V. The fact that irreversibility is observed in electrolytes of different nature (carbonates and AILs) at potentials above 1 V seems to discard electrolyte degradation as a cause for this irreversibility [42]. Recent studies on electrodes based on amorphous TiO_2 nanoparticles point to the importance of adsorbed H_2O/OH species to explain irreversibility after the first discharge curve [43]. Specifically, a Li_2O interface layer is established by reaction of adsorbed H_2O/OH species with the Li-ions coming from the electrolyte. In our electrodes, once discarded electrolyte degradation, the irreversibility could also be associated with the formation of a Li_2O SEI layer by reaction with remaining OH species. On the basis of this interpretation, the higher irreversibility shown in the porous mesocrystals when compared to non-porous 25 nm commercial samples (Fig. 3), could be explained by the higher surface area of porous mesocrystals (i.e. higher concentration of OH species). Impedance measurements (Nyquist plots in Fig. S2 of Supplementary information) also suggest the presence of a SEI. Specifically after cycling the plots showed an additional semicircle often interpreted as coming from the relaxation of charge carriers in a solid electrolyte interphase [44].

Finally, the differences in capacity at full discharge when comparing anodes in ionic liquid electrolytes with those in carbonates (Fig. 3) can come from the specifics of the SEI with possible contributions from limited lithium-ion transport through the electrolyte, as we better describe in the next section.

3.3. Rate capability performance

As above-mentioned, a common factor in all the battery studies using AILs is that limited lithium-ion transport becomes a substantial issue at high rates. Indeed, the specific capacity at 67 mA g^{-1} (Fig. 4) is among the best values reported for anatases in organic carbonates [29,33,34,37,40]. However, as the current rate increases, the performance in AILs electrolytes worsens because the electrolyte cannot provide lithium-ions at sufficient rate (Fig. 4). Still, the performance is better than that for 25 nm commercial nanoanatases in ionic liquids, and even at 336 mA g^{-1}, the mesocrystal/ionic liquid combination gives a capacity at full discharge similar to the 25 nm commercial sample/organic carbonate combination (Fig. 4). Supporting the argument of limited lithium-ion transport through the electrolyte, the lithium diffusion coefficient measured by NMR for the AIL electrolyte was lower than for carbonates (8.3×10^{-12} vs. $2{,}1 \times 10^{-10}$ m^2 s^{-1}). Moreover, the increase in rate capability performance at 60 °C for the mesocrystals in the AILs (Fig. 4) can again be linked to an increase in the lithium diffusion coefficient (2.0×10^{-11} at 60 °C vs. 8.3×10^{-12} m^2 s^{-1}). Interestingly, the specific capacity at full discharge for the mesocrystals in AILs when compared to the above-mentioned nanotubes at comparable rates is similar (190 vs. 180 mAh g^{-1} for nanotubes at ~65 mA g^{-1}; 150 vs. 145 mAh g^{-1} for nanotubes at ~170 mA g^{-1}) [17]. These results confirm the good accessibility and wettability of the mesocrystals, and furthermore their relatively good performance because as above-mentioned the intrinsic free volume (nanotube interior vs. mesocrystal mesoporosity) is lower for the mesocrystals (ca. 40% vs. ca. 70% for nanotubes).

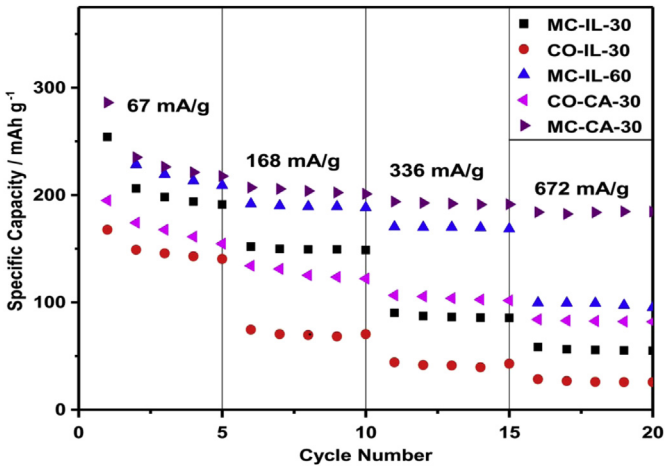

Fig. 4. Rate capability performance at full discharge for mesocrystals in ionic liquids measured at 30 and 60 °C (MC-IL-30, MC-IL-60), mesocrystals in carbonates at 30 °C (MC-CA-30) and for commercial anatases in ionic liquids (CO-IL-30) and carbonates (CO-CA-30) at 30 °C. Importantly, measurements at 60 °C were registered after the 30 °C treatment.

3.4. Temperature stability studies

As previously mentioned, the main objective of the research here presented is to explore possible pathways for safer LiBs working with liquid electrolytes over a wide temperature window (of special interest are temperatures above 50–60 °C). As both anatase anodes and AIL electrolytes are intended for applications in which safety, durability and variability in operating temperature represent the primary concerns, the results from Fig. 4 clearly suggest that in order to preserve a high but yet stable electrochemical performance over a wide temperature range, galvanostatic experiments at higher temperatures must be carried out at 67 mA g^{-1}. Thus, temperature stability studies were carried out at this rate and only for the porous mesocrystals, as they clearly outperform the commercial samples in both specific capacity and rate capability figures-of-merit (Figs. 3 and 4). Indeed at room temperature the porous mesocrystals in carbonate electrolytes showed better performance than that in AILs electrolytes (Figs. 3 and 4). However, at 60 °C AIL electrolytes clearly outperform carbonates (Fig. 5). Thus, after 62 cycles (~15 days for the AIL and ~13 days for carbonates), the AILs still retain a capacity of 185 mAh g^{-1} while in carbonates lowers down to 100 mAh g^{-1} (80 mAh g^{-1} in terms of similar operating time, ~15 days or 81 cycles). Furthermore, in Fig. 5 we show that the performance is still remarkable for a TiO_2-based anode even after extending the treatment for another 15 days at 80 °C (71 cycles + 62 cycles at 60 °C for a total of ca. 130 cycles) in the AILs electrolytes (155 mAh g^{-1} or 200 mAh cm^{-3}) with a coulombic efficiency of ca. 99% (Fig. 5).

4. Conclusions

In summary, we have shown that monodisperse TiO_2 anatase mesoporous colloidal mesocrystals, synthesized by a self-assembly/seeding assisted method, can be easily processed as active materials in anode composites. These anode composites can be efficiently infiltrated with safe ionic liquid electrolytes down to the mesocrystals' mesoporosity, and operate over a wide temperature window (of special interest are temperatures above 50–60 °C). For example, after continuous galvanostatic cycling for 1 month at high temperatures (15 days at 60°C + 15 days at 80 °C, ca. 130 cycles), these anode composites sustain a capacity (155 mAh g^{-1} or 200 mAh cm^{-3} with a coulombic efficiency of ca. 99% at 67 mA g^{-1}) that is still remarkable for TiO_2-based anodes. On contrast, in organic carbonates the capacity decays down to 80 mAh g^{-1} after only 15 days at 60 °C. Our results indicate that the principles derived from porous anatase mesocrystal/ionic liquid electrolyte combinations could constitute the basis for battery applications in which safety, durability and variability in operating temperature represent the primary concerns. On the basis of these principles we understand that further optimization relies on three more or less important approaches: a) development of new formulations for ionic liquids to overcome limited lithium transport (for example the above-mentioned recently reported protic ionic liquids [11,12]); b) optimization of the free volume left by both the anatase and the composite electrode and c) to reduce the aggregate size either by changing processing parameters or by applying more sophisticated processing routes.

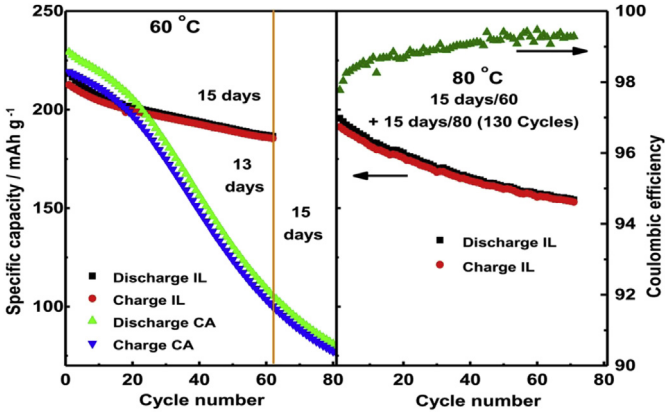

Fig. 5. (LEFT) Specific capacity at full discharge/charge for ionic liquids and carbonates as a function of cycles number measured at 60 °C (current rate of 67 mA g^{-1}) after SEI formation. (RIGHT) For the ionic liquids, after cycling for 15 days at 60 °C, the temperature was raised to 80 °C and the specific capacity along with the coulombic efficiency was measured for another 15 days (71 cycles + 62 cycles from 60 °C). Finally, it is worthy noting that in galvanostatic tests with a fixed voltage window, the time it takes for a cycle to be completed shortens as the capacity declines, and so the number of cycles for a given period of time does not match in samples with different lost.

Acknowledgment

Financial support from projects MAT2011-22969 and MAT2011-25198 is gratefully acknowledged. P.T thank the staff of ICTS Centro Nacional de Microscopía Electrónica of the Complutense University of Madrid (UCM) for kindly providing technical support.

Appendix A. Supplementary data

Supplementary data related to this article can be found at http://dx.doi.org/10.1016/j.jpowsour.2014.09.106.

References

[1] G.T. Kim, S.S. Jeong, M. Joost, E. Rocca, M. Winter, S. Passerini, A. Balducci, J. Power Sources 196 (2011) 2187.
[2] G.-T. Kim, S.S. Jeong, M.-Z. Xue, A. Balducci, M. Winter, S. Passerini, F. Alessandrini, G.B. Appetecchi, J. Power Sources 199 (2012) 239.
[3] Q. Wang, P. Ping, X. Zhao, G. Chu, J. Sun, C. Chen, J. Power Sources 208 (2012) 210.
[4] Z. Chen, I. Belharouak, Y.-K. Sun, K. Amine, Adv. Funct. Mater. 23 (2013) 959.
[5] J.S. Lee, J.Y. Bae, H. Lee, N.D. Quan, H.S. Kim, H. Kim, J. Ind. Eng. Chem. 10 (2004) 1086.
[6] N.D. Petkovich, S.G. Rudisill, B.E. Wilson, A. Mukherjee, A. Stein, Inorg. Chem. 53 (2014) 1100.
[7] R. Hagiwara, J.S. Lee, Electrochemistry 75 (2007) 23.
[8] A. Lewandowski, A. Świderska-Mocek, J. Power Sources 194 (2009) 601.
[9] C. Ding, T. Nohira, K. Kuroda, R. Hagiwara, A. Fukunaga, S. Sakai, K. Nitta, S. Inazawa, J. Power Sources 238 (2013) 296.
[10] R.-S. Kühnel, N. Böckenfeld, S. Passerini, M. Winter, A. Balducci, Electrochim. Acta 56 (2011) 4092.
[11] N. Bockenfeld, M. Willeke, J. Pires, M. Anouti, A. Balducci, J. Electrochem. Soc. 160 (2013) A559.
[12] T. Vogl, S. Menne, R.-S. Kühnel, A. Balducci, J. Mater. Chem. A 2 (2014) 8258.
[13] J.-H. Shin, W.A. Henderson, S. Passerini, Electrochem. Commun. 5 (2003) 1016.
[14] M. Egashira, M. Tanaka-Nakagawa, I. Watanabe, S. Okada, J. Yamaki, J. Power Sources 160 (2006) 1387.
[15] M. Ishikawa, T. Sugimoto, M. Kikuta, E. Ishiko, M. Kono, J. Power Sources 162 (2006) 658.
[16] A. Guerfi, S. Duchesne, Y. Kobayashi, A. Vijh, K. Zaghib, J. Power Sources 175 (2008) 866.
[17] S. Ivanov, L. Cheng, H. Wulfmeier, D. Albrecht, H. Fritze, A. Bund, Electrochim. Acta 104 (2013) 228.
[18] H. Cölfen, M. Antonietti, Angew. Chem. Int. Ed. Engl. 44 (2005) 5576.
[19] J. Seto, Y. Ma, S.A. Davis, F. Meldrum, A. Gourrier, Y.-Y. Kim, U. Schilde, M. Sztucki, M. Burghammer, S. Maltsev, C. Jäger, H. Cölfen, Proc. Natl. Acad. Sci. U. S. A. 109 (2012) 3699.
[20] L. Zhou, P. O'Brien, J. Phys. Chem. Lett. 3 (2012) 620.
[21] T. Tachikawa, T. Majima, NPG Asia Mater. 6 (2014) e100.
[22] M.-G. Ma, H. Cölfen, Curr. Opin. Colloid Interface Sci. 19 (2014) 56.
[23] Y. Liu, Y. Zhang, J. Wang, CrystEngComm 16 (2014) 5948.
[24] P. Tartaj, J.M. Amarilla, Chem. Commun. (Camb.) 50 (2014) 2077.
[25] E.J.W. Crossland, N. Noel, V. Sivaram, T. Leijtens, J.A. Alexander-Webber, H.J. Snaith, Nature 495 (2013) 215.
[26] J. Popovic, R. Demir-Cakan, J. Tornow, M. Morcrette, D.S. Su, R. Schlögl, M. Antonietti, M.-M. Titirici, Small 7 (2011) 1127.
[27] J. Ye, W. Liu, J. Cai, S. Chen, X. Zhao, H. Zhou, L. Qi, J. Am. Chem. Soc. 133 (2011) 933.

[28] X. Duan, L. Mei, J. Ma, Q. Li, T. Wang, W. Zheng, Chem. Commun. (Camb.) 48 (2012) 12204.
[29] P. Tartaj, J.M. Amarilla, Adv. Mater. 23 (2011) 4904.
[30] E. Uchaker, G. Cao, Nano Today 9 (2014) 499.
[31] P. Tartaj, Chem. Commun. (Camb.) 47 (2011) 256.
[32] N. Serpone, D. Lawless, R. Khairutdinov, J. Phys. Chem. 99 (1995) 16646.
[33] Y. Ren, L.J. Hardwick, P.G. Bruce, Angew. Chem. Int. Ed. Engl. 49 (2010) 2570.
[34] G. Sudant, E. Baudrin, D. Larcher, J.-M. Tarascon, J. Mater. Chem. 15 (2005) 1263.
[35] Y.-G. Guo, Y.-S. Hu, W. Sigle, J. Maier, Adv. Mater. 19 (2007) 2087.
[36] K. Shen, H. Chen, F. Klaver, F.M. Mulder, M. Wagemaker, Chem. Mater. 26 (2014) 1608.
[37] H. Kim, M.G. Kim, J. Cho, Adv. Energy Mater. 2 (2012) 1425.
[38] C. Jiang, M. Wei, Z. Qi, T. Kudo, I. Honma, H. Zhou, J. Power Sources 166 (2007) 239.
[39] J. Wang, J. Polleux, J. Lim, B. Dunn, J. Phys. Chem.C 111 (2007) 14925.
[40] K. Zhu, Q. Wang, J.-H. Kim, A.A. Pesaran, A.J. Frank, J. Phys. Chem.C 116 (2012) 11895.
[41] P. Simon, Y. Gogotsi, B. Dunn, Science 343 (2014) 1210.
[42] L. Fei, Y. Xu, X. Wu, Y. Li, P. Xie, S. Deng, S. Smirnov, H. Luo, Nanoscale 5 (2013) 11102.
[43] W.J.H. Borghols, D. Lützenkirchen-Hecht, U. Haake, W. Chan, U. Lafont, E.M. Kelder, E.R.H. van Eck, A.P.M. Kentgens, F.M. Mulder, M. Wagemaker, J. Electrochem. Soc. 157 (2010) A582.
[44] J. Vetter, P. Novák, M.R. Wagner, C. Veit, K.-C. Möller, J.O. Besenhard, M. Winter, M. Wohlfahrt-Mehrens, C. Vogler, A. Hammouche, J. Power Sources 147 (2005) 269.